THE JOURNAL OF BIOLOGICAL CHEMISTRY VOL. 281, NO. 32, pp. 23254–23263, August 11, 2006

The Synthesis, Structural Characterization, and Receptor Specificity of the α-Conotoxin Vc1.1*

Received for publication, May 12, 2006 Published, JBC Papers in Press, June 5, 2006, DOI 10.1074/jbc.M604550200

Richard J. Clark[‡1], **Harald Fischer**[§1], **Simon T. Nevin**[§1], **David J. Adams**[§], **and David J. Craik**[‡2]

From the [‡]*Institute for Molecular Bioscience and* [§]*School of Biomedical Sciences, University of Queensland, Brisbane, Queensland 4072, Australia*

The α-conotoxin Vc1.1 is a small disulfide-bonded peptide currently in development as a treatment for neuropathic pain. This study describes the synthesis, determination of the disulfide connectivity, and the determination of the three-dimensional structure of Vc1.1 using NMR spectroscopy. Vc1.1 was shown to inhibit nicotine-evoked membrane currents in isolated bovine chromaffin cells in a concentration-dependent manner and preferentially targets peripheral nicotinic acetylcholine receptor (nAChR) subtypes over central subtypes. Specifically, Vc1.1 is selective for α3-containing nAChR subtypes. The three-dimensional structure of Vc1.1 comprises a small α-helix spanning residues Pro[6] to Asp[11] and is braced by the I–III, II–IV disulfide connectivity seen in other α-conotoxins. A comparison of the structure of Vc1.1 with other α-conotoxins, taken together with nAChR selectivity data, suggests that the conserved proline at position 6 is important for binding, whereas a number of residues in the C-terminal portion of the peptide contribute toward the selectivity. The structure reported here should open new opportunities for further development of Vc1.1 or analogues as analgesic agents.

Conotoxins are peptide toxins, ranging in size from 12 to 30 amino acids, isolated from the venom of snails from the *Conus* genus (1). Members of this peptide family target a range of membrane receptors with both high potency and selectivity and as a consequence are useful as neuropharmacological probes and have a range of potential pharmaceutical applications. The α-conotoxins are a subfamily of conotoxins that typically range in size from 12 to 16 amino acids, which contain two disulfide bonds in a I–III, II–IV connectivity and have an amidated C terminus. The α-conotoxins interact with both muscle and neuronal nicotinic acetylcholine receptors (nAChRs),[3] which have been implicated in a range of disorders, including Alzheimer disease, schizophrenia, depression, and small cell lung carcinoma, and they play a role in analgesia and addiction (2–5). Selected α-conotoxin examples are shown below in Fig. 1.

The α-conotoxin Vc1.1 was first discovered using a PCR screen of cDNAs from the venom ducts of *Conus victoriae* (6). The cysteine spacing within the sequence of Vc1.1 suggests that it is a member of the 4/7 subclass of α-conotoxins, which includes the extensively studied conotoxins MII, EpI and PnIB, although the actual disulfide connectivity of Vc1.1 has yet to be reported. In addition to an amidated C terminus, which is common to all α-conotoxins, Pro[6] and Glu[14] in Vc1.1 are post-translationally modified to hydroxyproline and γ-carboxyglutamate, respectively. The post-translationally modified peptide, designated vc1a, was recently identified in the venom of *C. victoriae* using MS analysis (7).

Synthetic Vc1.1, an antagonist of neuronal nAChRs in bovine chromaffin cells, has been shown to alleviate neuropathic pain in three rat models of human neuropathic pain and to accelerate the functional recovery of injured neurons (8). As an analgesic, Vc1.1 has been reported be more active than ω-conotoxin MVIIA, a conotoxin that has recently been approved as a treatment for intractable pain (6). More recently, Vc1.1 was shown to antagonize the nicotine-induced increase in axonal excitability of unmyelinated C-fiber axons in isolated segments of peripheral human nerves (9). Electrophysiological and immunohistochemical data indicate the functional expression of nAChRs composed of α3, α5, and β4 but not α4, β2, or α7 subunits in axons of unmyelinated C fibers (9, 10). Blockade of nAChRs on unmyelinated peripheral nerve fibers may have an analgesic effect on unmyelinated sympathetic and/or sensory axons. Interestingly, synthetic vc1a was reported to not inhibit the neuronal-type nicotinic response in chromaffin cells and was inactive in two rat neuropathic pain assays (7). Vc1.1 is now under development as a treatment for neuropathic pain (5, 11) but neither a specific receptor target nor the structure has been reported.

Herein, we report the three-dimensional structure of Vc1.1 in solution as determined by NMR spectroscopy and explicitly determine the disulfide connectivity via chemical reduction and MS analysis. In addition, we show that Vc1.1 selectively antagonizes peripherally expressed nAChRs subtypes over

* This work was supported in part by funding from the Australian Research Council. The costs of publication of this article were defrayed in part by the payment of page charges. This article must therefore be hereby marked "*advertisement*" in accordance with 18 U.S.C. Section 1734 solely to indicate this fact.

The atomic coordinates and structure factors (code 2H8S) have been deposited in the Protein Data Bank, Research Collaboratory for Structural Bioinformatics, Rutgers University, New Brunswick, NJ (http://www.rcsb.org/).

[1] These authors contributed equally to this work.

[2] An Australian Research Council Professorial Fellow. To whom correspondence should be addressed. Tel.: 61-7-3346-2019; Fax: 61-7-3346-2029; E-mail: d.craik@imb.uq.edu.au.

[3] The abbreviations used are: nAChR, nicotinic acetylcholine receptor; ACh, acetylcholine; DQF-COSY, double quantum filtered correlated spectroscopy; RP-HPLC, reversed-phase-high performance liquid chromatography; IC_{50}, half-maximal inhibitory concentration; MS, mass spectrometry; MS/MS, tandem mass spectrometry; ES-MS, electrospray-mass spectrometry; NOE, nuclear Overhauser effect; NOESY, nuclear Overhauser effect spectroscopy; TOCSY, total correlation spectroscopy; MES, 2-morpholinoethanesulfonic acid; r.m.s.d., root mean square deviation.

those typically expressed in the central nervous system. These findings provide an insight into the potential modes of action of this analgesic peptide. We also examined the structure and activity of two derivatives of Vc1.1, vc1a and [P6O]-Vc1.1, which contain the post-translationally modified residues hydroxyproline and γ-carboxyglutamic acid and compare them to our findings for Vc1.1.

EXPERIMENTAL PROCEDURES

Peptide Synthesis and Oxidative Folding—Vc1.1, vc1a, and [P6O]-Vc1.1 were assembled on 4-methylbenzhydrylamine amide resin (Auspep) by manual solid-phase peptide synthesis using the *in situ* neutralization/*O*-benzotriazole-*N*,*N*,*N*′,*N*′-tetramethyluronium hexafluorophosphate protocol for *t*-butoxycarbonyl chemistry (12). Cleavage of the peptide from the resin was achieved using HF with *p*-cresol and *p*-thiocresol as scavengers (9:0.5:0.5 (v/v) HF:*p*-cresol:*p*-thiocresol). The reaction was allowed to proceed at −5 to 0 °C for 1.5 h. The HF was then removed under vacuum, and the peptide was precipitated with ether, filtered, dissolved in 50% acetonitrile containing 0.05% trifluoroacetic acid, and lyophilized. The crude peptides were purified by RP-HPLC on a Phenomenex C_{18} column using a gradient of 0–80% B (Buffer A: H_2O/0.05% trifluoroacetic acid; Buffer B: 90% CH_3CN/10% H_2O/0.045% trifluoroacetic acid) in 80 min, and the eluant was monitored at 230 nm. These conditions were used in subsequent purification steps. Analytical RP-HPLC and ES-MS confirmed the purity and molecular mass of the synthesized peptides. The linear peptides were oxidized by dissolving in 0.1 M NH_4HCO_3 (pH 8.2) at a concentration of 0.3 mg/ml and stirring overnight at room temperature. The oxidized peptides were then purified by RP-HPLC, and the molecular weight was confirmed by ES-MS.

Determination of Disulfide Connectivity—Peptide (50 μg) was dissolved in 50 μl of 0.2 M sodium citrate (pH 3.0), and 50 μl of 20 mM *tris*-carboxyethylphosphine in citrate buffer was added. The reaction mixture was incubated at 37 °C for 5 min before injection onto the RP-HPLC. The partially reduced peptide was collected, and an equal volume of 20 mM *N*-ethylmaleimide in citrate buffer was added immediately. The reaction mixture was then incubated at 60 °C for 1 h, and the resulting product was isolated by RP-HPLC and lyophilized. The peptide was then redissolved in citrate buffer and fully reduced with an excess of *tris*-carboxyethylphosphine, resulting in a peptide with two free cysteines and two alkylated cysteines. This peptide was then analyzed by MS/MS sequencing to identify the location of the alkylated cysteines in the sequence.

NMR Spectroscopy—NMR data for Vc1.1, vc1a, and [P6O]-Vc1.1 were recorded on samples dissolved in 90% H_2O/10% D_2O at pH 3.5. Bruker ARX 500- and 600-MHz spectrometers were used in the acquisition of data. 2D NMR experiments included DQF-COSY, E-COSY, TOCSY, and NOESY, with all spectra recorded at 280 K. A series of 1D and TOCSY spectra acquired immediately following dissolution of fully protonated Vc1.1 in D_2O were used in the determination of slow exchanging NH protons. All spectra were analyzed on Silicon Graphics Indigo workstations using XWINNMR 1.3 (Bruker) and Sparky software. Chemical shifts were referenced to 2,2-dimethyl-2-silapentane 5-sulfonate at 0 ppm.

Structure Calculations on Vc1.1—Distance information for Vc1.1 was obtained from a NOESY spectrum with a mixing time of 200 ms at 280 K. Peak heights were used to determine distance restraints. Backbone dihedral restraints were determined from $^3J_{HN\text{-}H\alpha}$ coupling constants obtained from lineshape analysis of the anti-phase cross-signal splitting in a high digital resolution 2D DQF-COSY spectrum or from a 1D ^1H NMR spectrum. The ϕ angle was restrained to 120 ± 30° for $^3J_{HN\text{-}H\alpha} > 8$ Hz and −60 ± 30° for $^3J_{HN\text{-}H\alpha} < 5.8$ Hz. Intraresidue NOE and $^3J_{H\alpha\text{-}H\beta}$ coupling patterns were used in assigning χ^1 angle restraints of some side chains. There were also 12 restraints included for 6 hydrogen bonds identified from D_2O exchange data and preliminary structures.

Initial structures were generated using Dyana software (13), and the final structure calculations were performed using a simulated annealing protocol with CNS (14). This protocol involves a high temperature phase comprising 4000 steps of 0.015 ps of torsion angle dynamics, a cooling phase with 4000 steps of 0.015 ps of torsion angle dynamics during which the temperature is lowered to 0 K, and finally an energy minimization phase comprising 500 steps of Powell minimization. The resultant structures were subjected to further molecular dynamics and energy minimization in a water shell (15). The refinement in explicit water involved the following steps. First, heating to 500 K via steps of 100 K, each comprising 50 steps of 0.005 ps of Cartesian dynamics. Second, 2500 steps of 0.005 ps of Cartesian dynamics at 500 K before a cooling phase where the temperature is lowered in steps of 100 K, each comprising 2500 steps of 0.005 ps of Cartesian dynamics. Finally, the structures were minimized with 2000 steps of Powell minimization. Fifty structures were calculated, and the 20 with the lowest overall energies were retained for analysis. Structures were visualized using the program MOLMOL (16) and analyzed with PROMOTIF (17) and PROCHECK_NMR (18).

Electrophysiological Recordings from nAChRs in Bovine Adrenal Chromaffin Cells and Exogenously Expressed in Xenopus Oocytes—Chromaffin cells were prepared from bovine adrenal glands and maintained on glass coverslips in 24-well plates (Nunc) as previously described (19). Electrodes (GF150F-7.5, Harvard Apparatus Ltd., Edenbridge, UK) were pulled, fire-polished, and had resistances of 2–3 MΩ when filled with intracellular solution (in mM: 140 CsCl, 2 $CaCl_2$, 11 EGTA, 2 MgATP, 10 HEPES-KOH, pH 7.2). Agonists were diluted in bath solution (in mM: 140 NaCl, 3 KCl, 1.2 $MgCl_2$, 2.5 $CaCl_2$, 7.7 glucose, 10 HEPES-NaOH, pH 7.35) and were applied to cells by brief (10 ms) pressure ejection (15 p.s.i., Picospritzer II, General Valve, Fairfield, NJ) from an extracellular pipette positioned ~50 μm from the cell to evoke maximal responses to agonists (20). Conotoxins were bath applied and co-applied with the agonist in the extracellular pipette. Membrane currents evoked by agonist application were amplified and low pass filtered (10 kHz) using an MultiClamp 700B patch clamp amplifier (Axon Instruments Inc., Union City, CA), and voltage steps were generated from a PC Pentium computer using pCLAMP 9.2 software and a Digidata 1322A interface (Axon Instruments Inc.). All experiments were carried out at room temperature (22 °C).

RNA preparation, oocyte preparation, and expression of nAChR subunits in *Xenopus* oocytes were performed as

described previously (21). Briefly, plasmids with cDNA encoding the rat α1–α7, β1–4, γ, and δ nAChR subunits were provided by J. Patrick (Baylor College of Medicine, Houston, TX) and subcloned into the oocyte expression vector pNKS2. All oocytes were injected with 5 ng of cRNA, except the α5- and α6-containing nAChRs in which 15–20 ng of each subunit was injected to aid expression and then kept at 18 °C in ND96 buffer (96 mM NaCl, 2 mM KCl, 1 mM $CaCl_2$, 1 mM $MgCl_2$, and 5 mM HEPES, at pH 7.4) supplemented with 50 mg/liter gentamycin and 5 mM pyruvic acid 2–5 days before recording.

Membrane currents were recorded from *Xenopus* oocytes using an automated work station with eight channels in parallel, including drug delivery and on-line analysis (OpusXpress™ 6000A workstation, Axon Instruments Inc.). Both the voltage-recording and current-injecting electrodes were pulled from borosilicate glass (GC150T-15, Harvard Apparatus Ltd.) and had resistances of 0.3–1.5 MΩ when filled with 3 M KCl. All recordings were conducted at room temperature (20–23 °C) using a bath solution of ND96 as described above. HEPES (pK_a 7.48) was replaced by MES (pK_a 6.1) as the buffer in the bath solution for experiments carried out at pH 6.0. During recordings, the oocytes were perfused continuously at a rate of 1.5 ml/min, with 250-s incubation times for the conotoxin. Acetylcholine (100 μM) was applied for 2 s at 5 ml/min, with 600-s washout periods between applications. Cells were voltage-clamped at a holding potential of −80 mV. Data were sampled at 500 Hz and filtered at 200 Hz. Peak current amplitude was measured before and following incubation of the toxin.

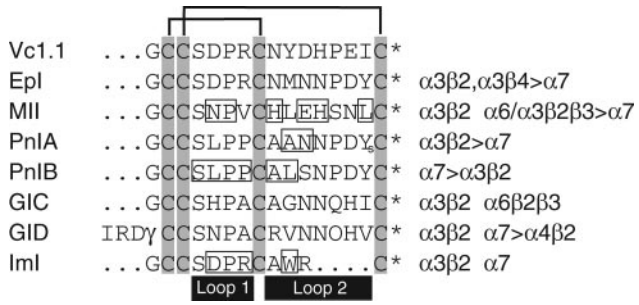

FIGURE 1. **Sequences of selected α-conotoxins, including Vc1.1.** Standard one letter codes are used, with *O* representing hydroxyproline, γ a γ-carboxyglutamic acid, and Y_s a sulfonated tyrosine. An *asterisk* indicates an amidated C terminus, which is a common post-translational modification of α-conotoxins. The common disulfide framework of I–III, II–IV is indicated at the *top*, and the conserved cysteines are *shaded*. The residues between Cys-II and Cys-III and Cys-III and Cys-IV are commonly referred to as *loops 1* and *2*, respectively, and are indicated by the *black bars* at the *bottom*. The number of residues in each of these loops is used to further classify the α-conotoxins. For example, Vc1.1 is classified as a 4/7 α-conotoxin, whereas ImI is a 4/3 α-conotoxin. The selectivity for nAChR subtypes of each conotoxin is shown on the *right*. Residues important for potency and/or selectivity are highlighted by a *box*. References to the various conotoxins are as follows: MII (44), EpI (39), PnIA (46), PnIB (46), GIC (47), GID (48), and ImI (49).

Statistics—All data represent arithmetic means ± S.E. Concentration-response curves for antagonists were fitted by unweighted non-linear regression to the logistic equation,

$$E_x = E_{max}X^n/(X^n + IC_{50}{}^n) \quad \text{(Eq. 1)}$$

where E_x is the response, X is the antagonist concentration, E_{max} is the maximal response, n is the slope factor, and IC_{50} is the concentration of antagonist that gives 50% inhibition of the agonist response. Computation was done using SigmaPlot 8.0 (Jandel Corp.).

The rate of onset and recovery from block during toxin washout were obtained from single exponential fits to the data using SigmaPlot 8.0. The K_d for the toxin was then calculated using Equation 2,

$$K_d = k_{off}/k_{on} \quad \text{(Eq. 2)}$$

where $k_{off} = 1/\tau_{off}$ (s^{-1}) and $k_{on} = (1/\tau_{on} - k_{off})/[\text{toxin}]$. The mechanisms of competitive antagonism were evaluated by means of the Schild regression (22),

$$\log(x - 1) = \log K_i - npA_x \quad \text{(Eq. 3)}$$

where pA_x is the negative logarithm of the concentration of the inhibitor, x is the shift of the concentration-response curve (dose ratio) caused by its presence, K_i is the dissociation constant of the inhibitor, and n is the slope factor. The regression line fitted to the data intersects the abscissa at a point corre-

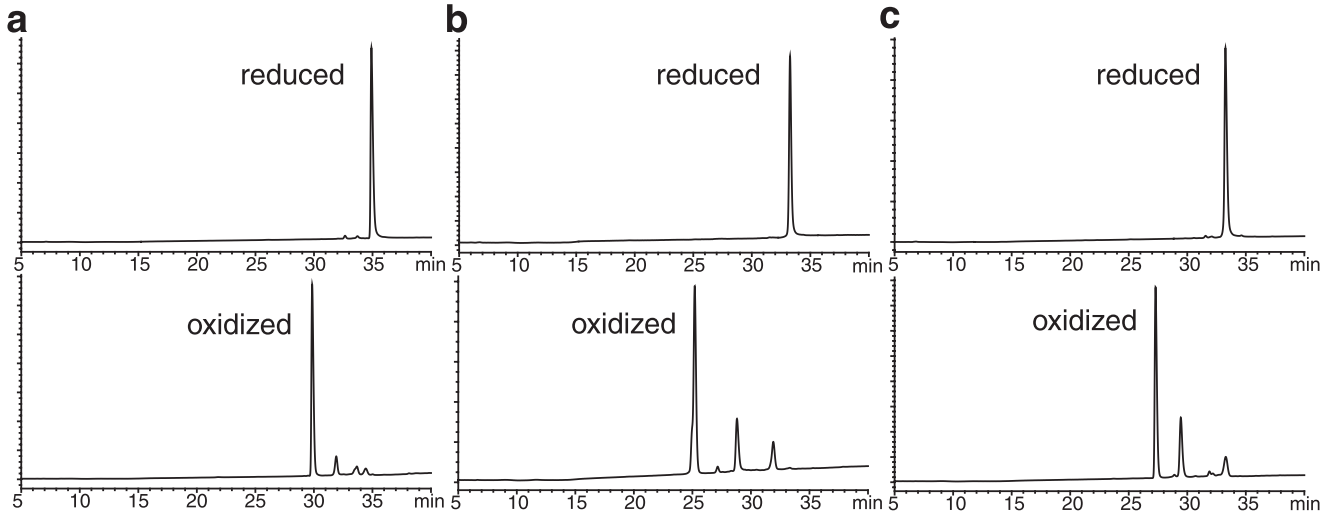

FIGURE 2. **HPLC profiles for the oxidation of Vc1.1 (*a*), vc1a (*b*), and [P6O]-Vc1.1 (*c*).** In each case, the *top trace* shows an RP-HPLC chromatogram of the reduced peptide. The *bottom trace* shows an RP-HPLC chromatogram of the oxidation mixture after incubation in 0.1 M NH_4HCO_3 for 24 h at room temperature. The disulfide connectivity of the major product for each peptide was confirmed as I–III, II–IV by partial reduction and MS/MS sequencing.

sponding to pA_2, which in the case of $n = 1$ corresponds to K_i (22).

RESULTS

Peptide Synthesis and Oxidative Folding—The sequence of Vc1.1 is shown in Fig. 1. The post-translationally modified derivative of Vc1.1, vc1a, which is found in the venom, contains a hydroxyproline in position 6 and a γ-carboxyglutamic acid in position 14. To further define the roles of these modified residues a third peptide, [P6O]-Vc1.1, was made that contained a hydroxyproline in position 6 but retained the unmodified glutamic acid at position 14. Vc1.1, vc1a, and [P6O]-Vc1.1 were synthesized using *t*-butoxycarbonyl/*in situ* neutralization chemistry on 4-methylbenzhydrylamine amide resin. The overall yield of reduced peptides based on the initial starting resin was ~30%. The oxidation profile of the peptides in 0.1 M NH_4HCO_3 buffer are shown in Fig. 2. All three peptides, Vc1.1, vc1a, and [P6O-Vc1.1, formed almost exclusively a single isomer with a monoisotopic molecular weights of 1809.7, 1866.6, and 1821.6, respectively, determined by ES-MS.

Disulfide Mapping of Vc1.1—Vc1.1, vc1a, and [P6O]-Vc1.1 were partially reduced by incubating with *tris*-carboxyethylphosphine in citrate buffer at low pH. The reaction mixture was purified by RP-HPLC, and the one-disulfide species was alkylated with *N*-ethylmaleimide. The alkylated peptide was then fully reduced and analyzed by MS/MS. For all three peptides the MS/MS data clearly showed that C2 and C8 had been alkylated with *N*-ethylmaleimide. Fragmentation patterns from both ends of the peptide chain were observed and fully supported the proposed alkylation pattern. Therefore, it was concluded that the disulfide connectivity of Vc1.1, vc1a, and [P6O]-Vc1.1 was C2 to C8 and C3 to C16. This is consistent with the I–III, II–IV disulfide bonding pattern seen in other α-conotoxins.

NMR Analysis—NH-NH_{i+1}, Hα-NH_{i+1}, and Hβ-NH_{i+1} connectivities obtained from the NOESY spectrum were used in the sequential assignment of the individual spin systems determined from the TOCSY spectrum. Sequential Hα-NH_{i+1} connectivities in all three peptides were observed for the entire peptide chain except at Pro^6 and Pro^{13}. Hα-$H\delta_{i+1}$ connectivities were utilized in the assignment of these proline residues and incidentally confirmed that the X-Pro bonds were in the *trans* configuration. Analysis of chemical shift data indicated that residues Cys^2–Ser^4, P/O^6–Asp^{11}, and Pro^{13}–Cys^{16} all have a negative secondary shifts (Fig. 3*a*), indicating helical character. This is further supported by the small $^3J_{\alpha N}$ coupling constants observed for Vc1.1 and the slow D_2O exchange of the amide resonances for many of these residues (Fig. 3*c*). This predominance of helical character is characteristic of other α-conotoxin structures reported to date (4). Fig. 3 (*a* and *b*) illustrates the high degree of structural similarity between the three molecules. The secondary shifts are almost identical except for where there is a change in residue type at positions 6 and/or 14. This similarity in structure is reinforced by the fact the secondary shift for [P6O]-Vc1.1 matches vc1a at position 6 (as both share a hydroxyproline at this position) and matches Vc1.1 at position 14 (both Glu). A comparison of the chemical shift differences between the Hβ protons, shown in Fig. 3*b*, suggests that the side-chain orientations in each molecule are also very similar. Therefore, any differences in biological activity between the three peptides is most likely due to changes in the nature of the side chains rather than structural perturbations.

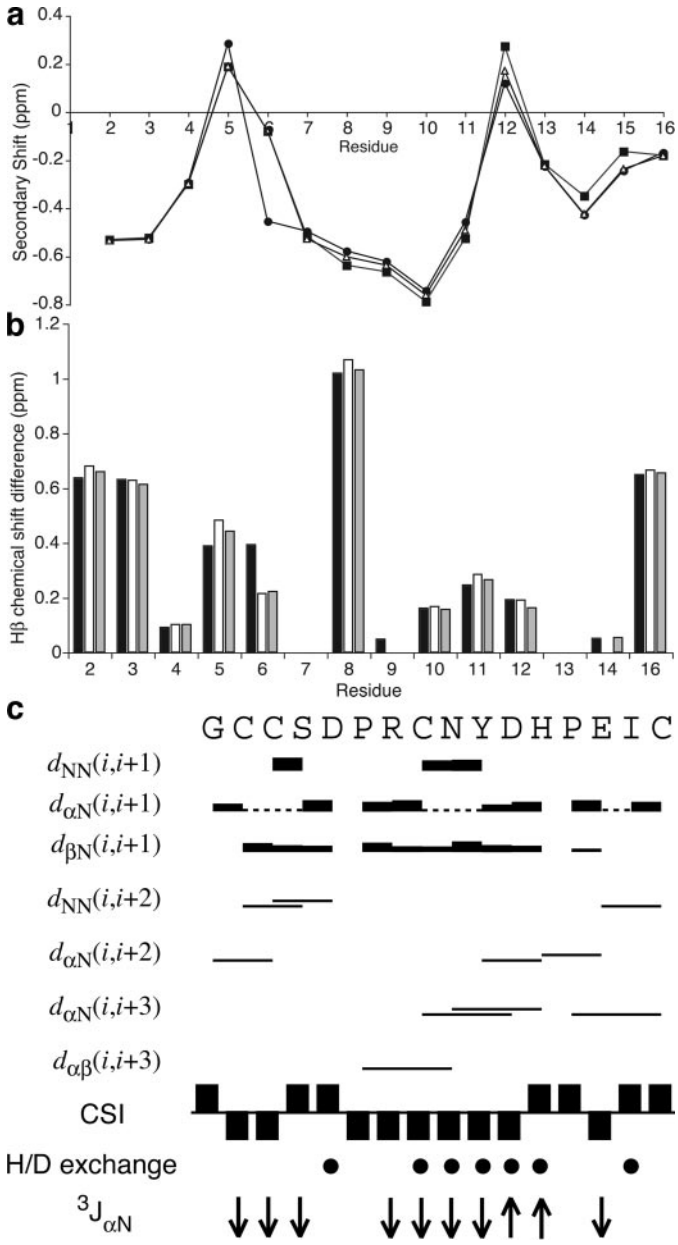

FIGURE 3. **A comparison summary of the NMR data for Vc1.1, vc1a, and [P6O]-Vc1.1.** *a*, secondary shift values for Vc1.1 (*filled circles*), vc1a (*filled squares*), and [P6O]-Vc1.1 (*open triangles*). The values for each peptide are almost identical indicating that the three-dimensional structures are very similar. *b*, a comparison of the chemical shift difference between Hβ protons for Vc1.1 (*black*), vc1a (*white*), and [P6O]-Vc1.1 (*gray*) indicating that the orientations of the side chains in each peptide are comparable. *c*, summary of coupling constants, chemical shift index, amide exchange and sequential-, medium-, and long-range NOE connectivities for Vc1.1. *Solid bars* represent sequential NOE connectivities observed in a 200-ms NOESY spectrum from a 500-MHz spectrometer at 280 K. The *height* of the *bar* represents the strength of the NOE cross-peak, classified as either strong, medium, or weak. $^3J_{NH\text{-}H\alpha}$ coupling constants ≥ 8 Hz (−120°) are represented as *upward arrows*, and coupling constants ≤ 5 Hz (60°) are represented as *downward arrows*. *Filled circles* indicate slow exchanging amide protons still present 30 min after dissolution in ^2H_2O at 298 K. Chemical shift indices (50) were derived from Hα chemical shifts of Vc1.1. An index of −1 or +1 indicates a shift deviation from the random coil value of >0.1 ppm upfield or downfield, respectively.

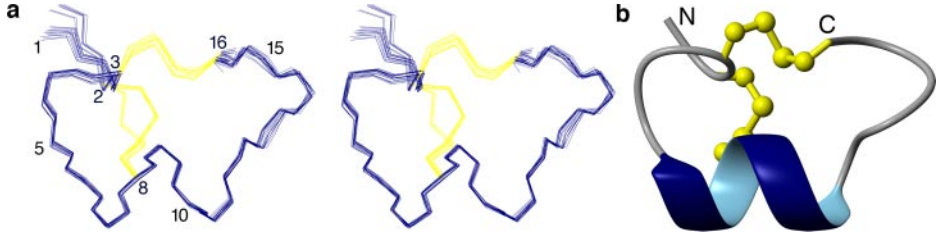

FIGURE 4. **The three-dimensional structure of Vc1.1.** *a*, stereoview of an ensemble of 20 low energy structures of Vc1.1 superimposed over all the backbone N, Cα, and C atoms. Every fifth residue, and the cysteines are numbered. *b*, ribbon representation of the average structure of Vc1.1 showing the helical region between residues Pro[6] and Asp[11]. Disulfide bonds are shown in *yellow* in *ball-and-stick* representation, and the N and C termini are marked.

TABLE 1
Energy and structural statistics for the family of 20 structures representing the solution structures of Vc1.1

Energies (kcal/mol)	
Overall	−623 ± 15
Bond	2.52 ± 0.34
Angle	15.4 ± 2.3
Improper	3.57 ± 0.70
van der Waals	−27.7 ± 4.3
NOE	3.55 ± 1.22
cDih	0.992 ± 0.267
Dihedral	54.5 ± 6.2
Electrostatic	−676 ± 20
R.m.s.d.	
Bond (Å)	0.003 ± 0.0002
Angle (degrees)	0.49 ± 0.04
Improper (degrees)	0.43 ± 0.04
NOE	0.025 ± 0.004
cDih	0.89 ± 0.12
Pairwise r.m.s.d.	0.32 ± 0.13
Backbone/heavy (Å)	1.32 ± 0.37
Experimental data	
Distance restraints	92
Dihedral restraints	21
NOE violations exceeding 0.20 Å	0
cDih violations exceeding 2.0°	0
Ramachandran	
Most favored (%)	91.7
Additionally allowed (%)	8.3

Structure Determination of Vc1.1—The solution structure of Vc1.1 was determined by simulated annealing using experimental distance restraints based on NOESY cross-peaks and dihedral angle restraints based on coupling constants. The restraints comprised 21 dihedral angle and 92 distance restraints, which included 59 sequential, 28 medium range, and 5 long range NOEs. Fifty structures were calculated, and the 20 lowest energy structures were chosen as representatives of the solution structure of Vc1.1 as shown in Fig. 4*a*. A summary of the energetic and geometric statistics for the family of structures is given in Table 1. The structures are in excellent agreement with the experimental data, showing no distance violation >0.2 Å and no dihedral angle violation >2°.

In general, the fold of Vc1.1, shown in Fig. 4, is consistent with that seen in other α-conotoxins. The main secondary structural element is an α-helix spanning residues Pro[6] to Asp[11]. In addition, PROMOTIF (17) recognizes a type I β-turn at the N terminus of the peptide for residues Cys[2] to Ser[4]. In 7 out of the 20 structures in the ensemble the 2–8 disulfide of Vc1.1 is defined as a right-hand hook conformation (χ_2 +ve, χ_3 +ve, χ_2' −ve), and in the remaining structures (13 of 20) the conformation is not formally classified by PROMOTIF (χ_2 +ve, χ_3 −ve, χ_2' −ve). In all 20 structures the 3–16 disulfide bond is in a left-hand spiral conformation. A comparison of the 2–8 disulfide bond in Vc1.1 with the crystal structures of [A10L,D14K]-PnIA and ImI in complex with the acetylcholine-binding protein (AChBP) (23) shows that the 2–8 disulfide of both peptides is similar to that of the 2–8 disulfide of Vc1.1 (*i.e.* χ_2 +ve, χ_3 −ve, and χ_2' −ve).

Potency of α-Conotoxin Vc1.1 at Native nAChRs—The functional activity of Vc1.1 was investigated via its effects on nicotine-evoked membrane currents in dissociated bovine chromaffin cells. Bath application of Vc1.1 reversibly inhibited nicotine (100 μM)-evoked depolarizing membrane currents in chromaffin cells voltage clamped at −100 mV (Fig. 5*a*). High micromolar concentrations (≥10 μM) of the toxin almost completely blocked the nicotine-evoked current in chromaffin cells, which recovered completely upon washout (Fig. 5*b*). Fig. 5*c* shows the concentration-response relationship obtained for inhibition of nicotine-evoked current amplitude by bath-applied Vc1.1. The curve fitted according to Equation 1 gave a half-maximal inhibitory concentration (IC_{50}) of 1.54 ± 0.14 μM and slope factor (Hill coefficient) of 1.64 ± 0.22 ($n = 6$). The time courses of onset of inhibition of nicotine-evoked current obtained in the presence of toxin and the recovery from block during toxin washout were fitted by single exponential functions. On- and off-rates of nAChR inhibition and estimates of potency (K_d) were obtained following application and washout of Vc1.1. Vc1.1 (10 μM) exhibited rapid onset of block ($k_{on} = 1.3 \pm 0.1 \times 10^3$ M^{-1} s^{-1}) and a maximum inhibition to 11 ± 2% ($n = 6$) of control. Recovery from block to 81 ± 4% ($n = 6$) of control was obtained after 10 min washout (Fig. 5*b*) and was associated with a dissociation rate constant, $k_{off} = 4.4 \pm 0.1 \times 10^{-3}$ M^{-1} s^{-1}. Therefore, using Equation 2, a K_d of 3.4×10^{-6} M was calculated.

Fig. 6*a* shows whole cell membrane currents evoked by focal application of 100 μM nicotine to the chromaffin cell held at different membrane potentials. Whole cell I–V relations obtained for peak nicotine-evoked currents obtained in the absence and presence of 1 μM and 2.5 μM Vc1.1 are shown in Fig. 6*b*. Vc1.1 reversibly inhibited nicotine-evoked current amplitude by ≥ 53% and ≥ 77% ($n = 6$) at all membrane potentials in the presence of 1 μM and 2.5 μM Vc1.1, respectively, indicating that the block of nAChRs by Vc1.1 was voltage-independent.

Competitive antagonism of nAChRs in chromaffin cells by Vc1.1 was evaluated from nicotine concentration-response relations determined in the absence and presence of various concentrations of Vc1.1. A rightward shift without noticeable depression of the concentration-response curve was observed for nicotine-induced currents in the presence of 0.5 μM, 1 μM, and 2.5 μM Vc1.1 (Fig. 6*c*). Schild plots constructed from shifts (dose ratios) of nicotine concentration-response curves in the absence and presence of Vc1.1 revealed pA_2 values of 6.33 (Fig. 6*d*). The slope of the Schild regression did not significantly

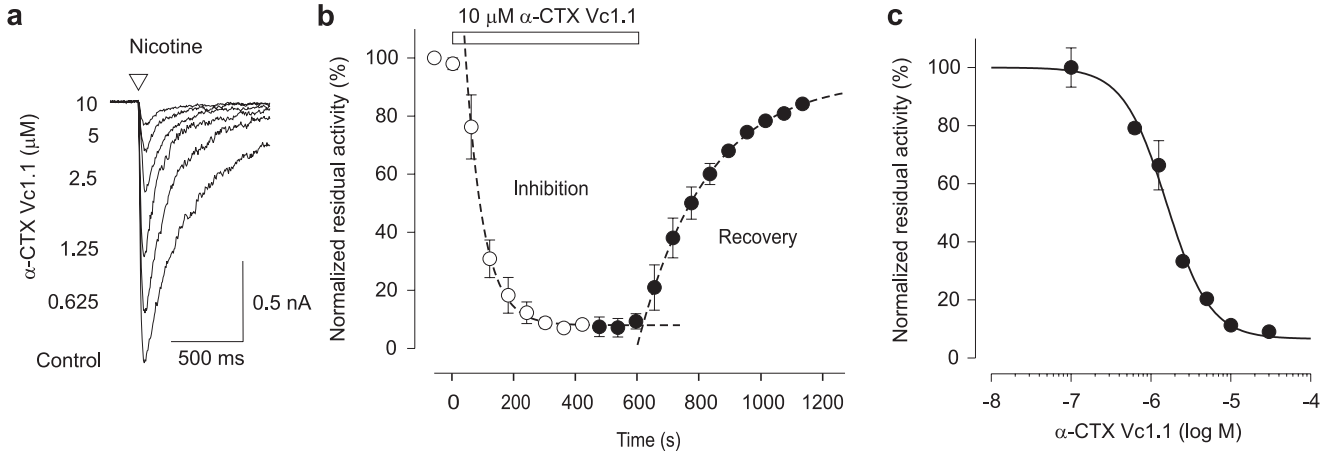

FIGURE 5. **Concentration dependence of Vc1.1 inhibition of nicotine-evoked currents in bovine adrenal chromaffin cells.** *a*, superimposed nicotine (100 μM)-evoked current traces recorded from isolated bovine chromaffin cells voltage-clamped at −100 mV in the absence and presence of different concentrations of Vc1.1 (as stated). *b*, normalized peak current amplitude as a function of time showing the onset (*open circles*) and recovery from block by Vc1.1 upon washout (*filled circles*). Current responses were evoked at 60-s intervals to minimize receptor desensitization. The toxin was applied as indicated. The onset and recovery from block were obtained from curve fits according to Equation 2 ($n = 4$). *c*, concentration-response relationship for the inhibition of nicotine evoked membrane currents from isolated bovine chromaffin cells by increasing concentrations of Vc1.1. Curve were fitted according to Equation 1.

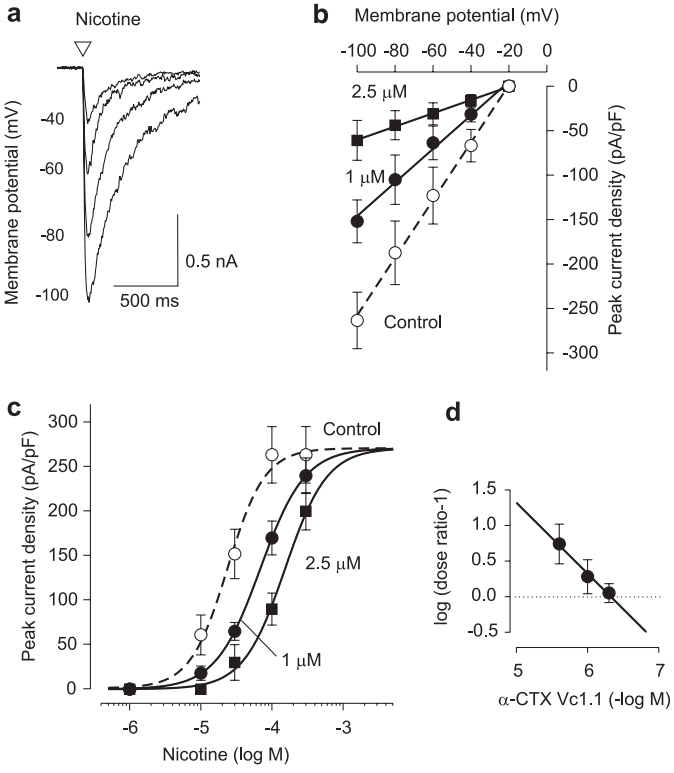

FIGURE 6. **Inhibition of nAChRs in bovine chromaffin cells by Vc1.1.** *a*, superimposed nicotine-evoked currents elicited by brief pulses (10 ms, as indicated by the *triangle*) of 100 μM nicotine from isolated chromaffin cells, voltage-clamped at membrane potentials from −100 to −40 mV in 20-mV increments. *b*, whole cell current-voltage relations obtained for peak current density (pA/picofarad) in the absence (control, *open circles*) and presence of 1 μM (*filled circles*) and 2.5 μM (*filled squares*) Vc1.1 bath applied. *c*, concentration-response relations of nicotine-evoked membrane currents from isolated chromaffin cells in the absence (control, *open circles*) and presence of 1 μM (*filled circles*) and 2.5 μM (*filled squares*) Vc1.1. Curves were fitted according to Equation 1. Curve shifts (dose ratios) caused by 0.5, 1, and 2.5 μM Vc1.1 were 2.1 ± 1.2, 2.9 ± 1.5, and 6.4 ± 1.6, respectively. Data are means ± S.E., $n = 4–6$ from three different preparations. *d*, Schild plot of dose ratios were calculated from curve shifts in the presence of a given concentration of the antagonist by fitting data points to Equation 1. The *line* fitted to the data has a slope of 0.99 ± 0.11 (S.E.), which does not significantly differ from unity and intersects the *dotted line* at 6.33 (pA_2 value, Equation 3).

differ from unity (−0.99), because the confidence interval of the estimate of the slope included 1 at the 5% significance level.

Selectivity of α-CTX Vc1.1 Inhibition of Recombinant nAChR Subtypes—Vc1.1 inhibition of ACh-induced currents was examined in *Xenopus* oocytes expressing various nAChRs subunit combinations. The ACh-evoked response was assessed every 10 min, and the toxin was bath-applied 4 min prior to co-application of the agonist plus toxin. Vc1.1 (10 μM) failed to inhibit ACh-evoked currents mediated by either the central nAChR subtypes, α4β2 and α4β4, or the skeletal muscle nAChR subtype, α1β1γδ ($n = 7–12$) (Fig. 7 and Table 2). Similarly, 10 μM Vc1.1 inhibited only 14 ± 2% of the ACh-evoked current mediated by the homopentameric neuronal nAChR, α7 ($n = 11$) (Fig. 7 and Table 2). However, 10 μM Vc1.1 inhibited the peripheral nAChR subtypes α3β2 and α3β4 to a similar extent, 58 ± 7% ($n = 8$) and 56 ± 7% ($n = 12$) of control, respectively. A similar potency was observed upon addition of the α5 subunit to the nAChR combination, α3α5β2 ($n = 7$), but Vc1.1 exhibited >5-fold lower potency to inhibit α3α5β4 ($n = 5$). Bath application of Vc1.1 at concentrations of ≤100 nM did not antagonize ACh-evoked currents nor elicit a detectable response alone (*i.e.* >50 nA) for α3-containing nAChRs. In a series of experiments, responses to ACh (100 μM) were measured before and after incubation with toxin at pH 7.4 and 6.0. Although extracellular acidification has been shown to inhibit neuronal nAChRs (24, 25), at pH 6.0, 1 μM Vc1.1 inhibited α3β4 by 44 ± 0.1% ($n = 4$), which was significantly more than that obtained at pH 7.4 (19 ± 0.1% inhibition) (data not shown).

The post-translationally modified peptides vc1a and [P6O]-Vc1.1 were also examined in *Xenopus* oocytes, under the same conditions as Vc1.1. Application of 10 μM vc1a or [P6O]-Vc1.1 failed to inhibit ACh-evoked currents mediated by α1β1γδ, α7, α4β4, α4β2, α3β4, and α3β2 nAChRs subunit combinations expressed in oocytes ($n = 4–9$). Higher concentrations of vc1a and [P6O]-Vc1.1 (30 μM) were also inactive on the α3β2 and α3β4 subtypes ($n = 2$) (data not shown).

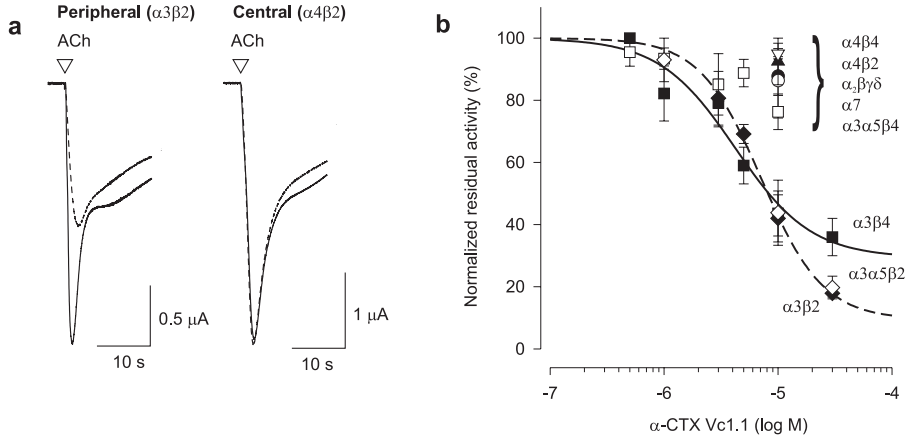

FIGURE 7. **Selectivity of Vc1.1 inhibition of nAChR subunit combinations expressed in *Xenopus* oocytes.** *a*, Vc1.1 (10 μM) inhibits 58 ± 8% ($n = 7$) of the ACh-evoked current amplitude mediated by α3β2 nAChRs but fails to inhibit α4β2 nAChRs expressed in oocytes. *b*, concentration-response curve of Vc1.1 inhibition of α3β2 receptors gave an IC_{50} of 7.3 μM (*filled diamonds*, $n_H = 1.7$) and 4.2 μM (*filled squares*, $n_H = 1.3$) for α3β4 receptors but only to a maximum of 71% inhibition. Addition of the α5 subunit for α3α5β2 receptors (*open diamonds*) did not change the IC_{50} (7.2 μM, $n_H = 1.3$) but reduced the potency of Vc1.1 for α3α5β4 receptors (*open squares*) by >5-fold. In contrast, Vc1.1 was >100-fold less potent on other nAChR subtypes: α7 (*open circles*), α1β1γδ (*filled circles*), α4β2 (*filled triangles*), and α4β4 (*open triangles*). Each data point represents the average of 4–7 oocytes. *Error bars* are ±S.E.

TABLE 2

α-Conotoxin Vc1.1 inhibition of recombinant nAChR subunit combinations expressed in *Xenopus* oocytes

nAChR subtype	IC_{50}	*n*	Hill slope	Maximum inhibition[a]
	μM			%
α3α5β2	7.2 ± 0.2	7	1.3 ± 0.3	94
α3β2	7.3 ± 0.7	12	1.7 ± 0.2	90
α3β4	4.2 ± 1.6	12	1.3 ± 0.6	70
α3α5β4, α4β2, α4β4, α7, and αβγδ	>30	5–12		<20

[a] Maximal inhibition was estimated from curves fitted to the data obtained at a maximum concentration of 30 μM.

DISCUSSION

In this study we have synthesized the α-conotoxin Vc1.1, determined its disulfide connectivity and three-dimensional structure, and identified its selectivity and potency for nAChR subtypes. The peptide was found to fold efficiently into one predominant isomer, which was subsequently determined to have a I–III, II–IV disulfide connectivity common to all α-conotoxins. These two disulfide bonds are the driving force for establishing the correct overall fold of the molecule and provide structural rigidity. Vc1.1 was shown to inhibit the nicotine-induced membrane current in bovine chromaffin cells in a concentration-dependent manner with a potency consistent with the observed inhibition of release of catecholamines (6). Moreover, Vc1.1 exhibited selectivity for α3-containing nAChRs, with similar potency for α3β2 and α3β4 nAChR subunit combinations. The potency of α3β2 was not altered by the addition of the α5 subunit, whereas the addition of the α5 subunit to α3β4 reduced the potency >5-fold. In contrast, Vc1.1 exhibited two-site displacement of [^{3}H]epibatidine from chromaffin cell membranes (K_i values of 2.3 nM and 3.7 μM), which suggests that Vc1.1 is a specific competitive inhibitor of one of the nAChR subtypes (6). Overall, Vc1.1 preferentially targets peripheral over central nAChR subtypes, but the difference between the radioligand binding and electrophysiological assays remains unresolved. The modified analogues vc1a and [P6O]-Vc1.1 did not inhibit ACh-evoked currents mediated by any of the nAChR subtypes expressed in *Xenopus* oocytes. The lack of activity of vc1a on neuronal nAChR subtypes is consistent with that reported previously in bovine chromaffin cells and rat models of neuropathic pain (26).

The three-dimensional structure of Vc1.1 reveals that it is a compact molecule dominated by a helical region over residues Pro^6 to Asp^{11}. The r.m.s.d. for the backbone atoms in the family of structures is 0.32 ± 0.13 Å, which indicates that the structure of the molecule is well defined. Overall, the three-dimensional fold of Vc1.1 is similar to those found for other 4/7 α-conotoxins. For example, a comparison of Vc1.1 with EpI (27), MII (28, 29), and PnIB (30) shows that the backbones overlay with r.m.s.d.s of only 0.47, 0.98, and 0.39 Å, respectively. A comparison of the NMR chemical shift data for vc1a and [P6O]-Vc1.1 with that for Vc1.1 showed that these two post-translationally modified analogues were structurally analogous to Vc1.1, and, therefore, the lack of biological activity of these two peptides was likely due to the side-chain modifications and not a structural perturbation. Notably, the surface properties of Vc1.1, shown in Fig. 8*a*, differ significantly from many other 4/7 α-conotoxins. This class of conotoxins typically has a patch of hydrophobic residues on one face that is believed to play a role in receptor binding and determining subtype specificity. It is clear from Fig. 8 that Vc1.1 has fewer hydrophobic residues on its surface than the α-conotoxins EpI (Fig. 8*b*) and MII (Fig. 8*c*), which are selective for the α3β4 and α3β2 nAChR subtypes, respectively.

Vc1.1 shares a number of common residues, apart from the conserved cysteines, with other α-conotoxins. The proline in position 6 is present in all α-conotoxins except for the recently discovered ImII, which acts at a different site on the nAChR (31). This proline residue has both a structural role and is also thought to contribute a key hydrophobic binding interaction with the β subunit of the nAChR (32). Recently, three crystal structures of α-conotoxins in complex with the AChBP have been published (23, 33, 34). All three structures reveal that loop 1 of the α-conotoxins, which includes Pro^6, is a key contributor to receptor binding. In the post-translationally modified analogue of Vc1.1, vc1a, Pro^6 is converted to a hydroxyproline and Glu^{14} is converted to a γ-carboxyglutamic acid (7). This modified peptide does not inhibit the nicotine-induced response in chromaffin cells (7), and we show here that this is due to a loss of activity at the α3β2 and α3β4 nAChR subtypes. One or both of these post-translational modifications must result in the loss of activity seen for vc1a, and it seems likely that the hydroxyproline is the major cause, because hydroxylation of this residue would dis-

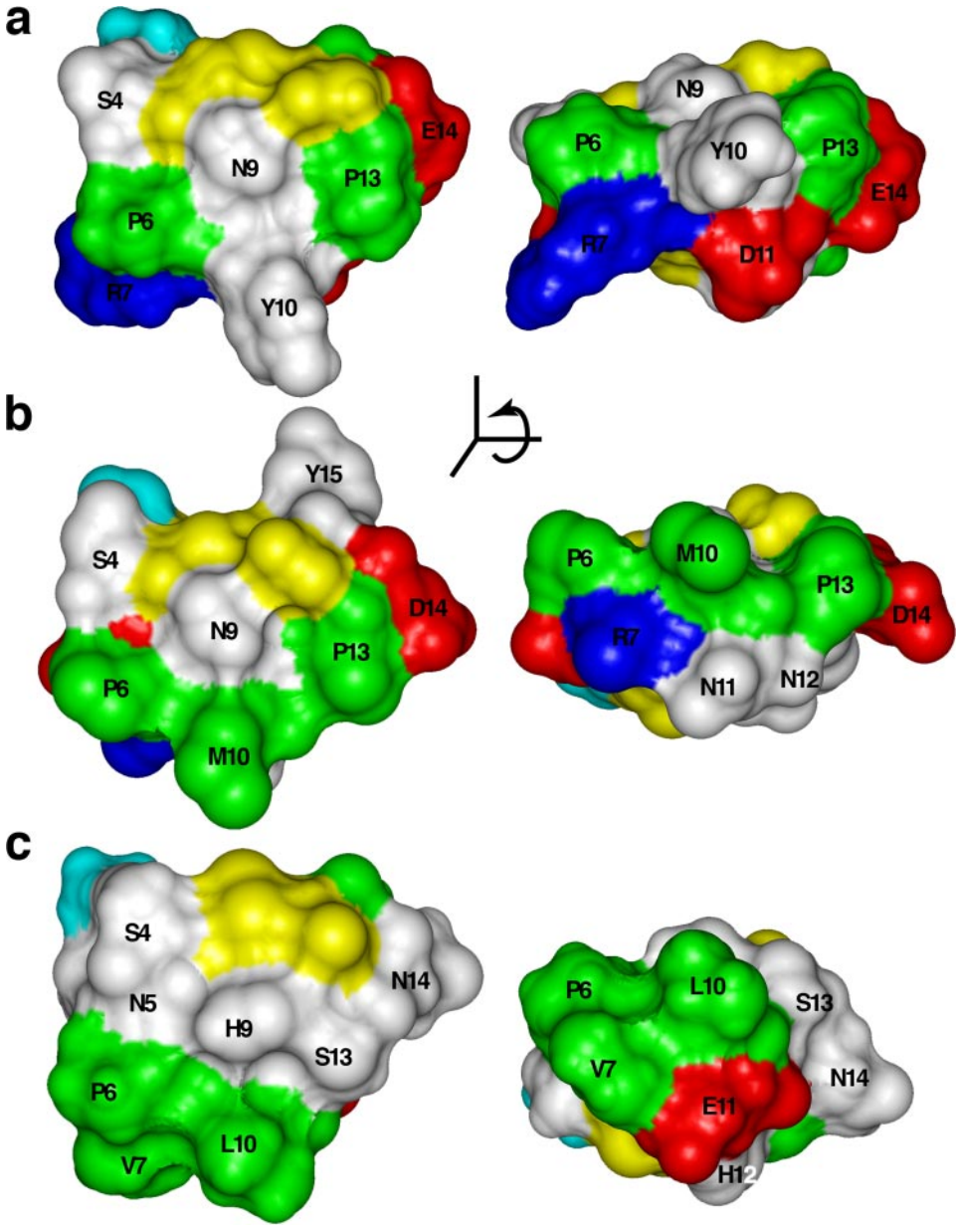

FIGURE 8. **Surface features of the α-conotoxins.** *a*, Vc1.1; *b*, EpI (PDB ID 1AOM); and *c*, MII (PDB ID 1MII). The surface image on the *right* for each conotoxin is rotated 90° around the *horizontal axis* with respect to the *left image*. Hydrophobic residues (Ala, Ile, Leu, Met, Pro, and Val) are shown in *green*, polar residues (Asn, His, Ser, Thr, and Tyr) are *white*, positive residues (Arg) are *blue*, negative residues (Asp and Glu) are *red*, glycine is *light blue*, and cystines are *yellow*. The histidine is assumed to be unprotonated at physiological pH. The structure of EpI is of the non-sulfonated tyrosine analogue.

rupt the conserved hydrophobic interactions with the nAChR. The key role of these interactions was confirmed by synthesis of [P6O]-Vc1.1, which has a hydroxyproline at position 6 but retains the glutamic acid at position 14. This peptide was also inactive on the nAChR and hence confirmed the key role of Pro^6 in the interaction of the conotoxin with the receptor, because presumably the presence of the hydroxyl group disrupts the hydrophobic interactions.

Fig. 9*a* shows the structure of Vc1.1 superimposed over the backbone of [A10L,D14K]-PnIA (backbone r.m.s.d. = 0.25 Å). The latter structure is derived from the crystal structure of [A10L,D14K]-PnIA, a 4/7 α-conotoxin, bound to the AChBP from *Aplysia californica* (23). The AChBP is a homologue of the extracellular ligand binding domain of the nAChR. As can be seen in Fig. 9*b* the highly conserved Pro^6 has hydrophobic interactions with both Trp^{145} and Tyr^{53}, whereas Glu^{14} is solvent-exposed and appears to be less important for the binding of the conotoxin to the receptor but may influence the selectivity of Vc1.1. This result is also consistent with a mutagenesis study on PnIB, which showed that substituting the proline at position 6 with a hydroxyproline resulted in a reduction in activity of ~15-fold at the α7 nAChR subtype (35).

In α-conotoxins it is generally found that the selectivity for α3β2 and α3β4 over the α7 nAChR subtype expressed in *Xenopus* oocytes is influenced by the length of the side chain of the hydrophobic residue at position 10, with longer extended aliphatic side chains tending to favor α7 selectivity (35–38). Vc1.1 has a tyrosine, relative to Val, Leu, Met, Ala, or Gly in other α-conotoxins, at position 10 and is selective for the α3β2 over the α7 nAChR subtype. The structure of Vc1.1 described here shows that the hydroxyl group of this tyrosine is surface-exposed, and therefore the combination of this hydroxyl group and the bulkier aromatic ring may disfavor interaction of Vc1.1 with the α7 nAChR subtype (Fig. 8*a*).

Vc1.1 has an identical sequence to EpI for the first nine residues, *i.e.* GCCSDPRCN but differs in five of the seven C-terminal residues. The sequence similarity is reflected in the surface characteristics of the two peptides shown in Fig. 8. The surfaces of the N-terminal portion of Vc1.1 (Fig. 8*a*) and EpI (Fig. 8*b*) exhibit a very similar distribution of hydrophobic, polar, and charged residues. EpI is a potent inhibitor of nAChRs in both bovine chromaffin cells and rat parasympathetic neurons that are rich in α3β4 and α3β2 subtypes, respectively (39). However, EpI inhibits rat α7 nAChR subtypes expressed in oocytes and has little effect on oocyte-expressed α3β2 and α3β4 subtypes (38). Although Vc1.1 shows negligible activity at the α7 nAChR subtypes expressed in oocytes, it is active in inhibiting nicotine-induced membrane currents and catecholamine release from bovine chromaffin cells and is active on α3β2 and α3β4 nAChR subtypes expressed in oocytes. This suggests that the differences in activity for EpI and Vc1.1 at the rat α7 nAChR subtype

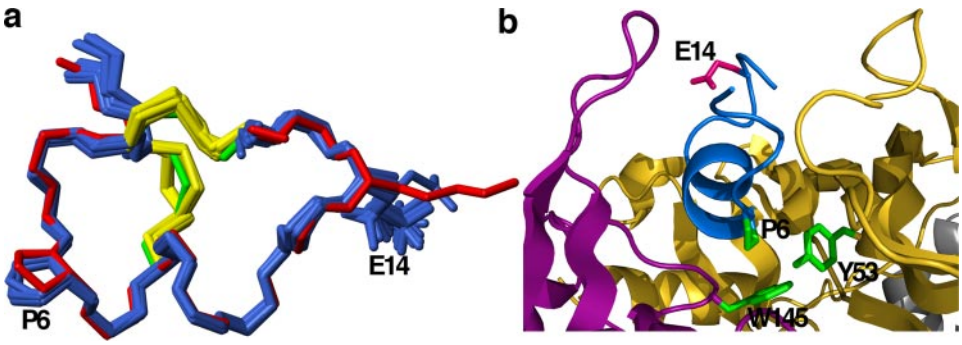

FIGURE 9. **A comparison of the crystal structure of [A10L,D14K]-PnIA bound to AChBP (23) with the structure of Vc1.1.** *a*, an overlay of the Vc1.1 NMR ensemble (*blue*) with the x-ray structure of [A10L,D14K]-PnIA (*red*) bound to AChBP illustrating the similarity in side-chain conformations at positions 6 and 14. Disulfide bonds are shown in *yellow* (Vc1.1) and *green* ([A10L,D14K]-PnIA). *b*, a ribbon representation of Vc1.1 (*blue*) within the binding pocket of AChBP (principle side in *purple* and complementary side in *yellow*). The backbone of Vc1.1 has been overlaid with that of [A10L,D14K]-PnIA (not shown) to illustrate the potential binding mode of Vc1.1. Pro^{6} of Vc1.1 (*green*) would potentially have hydrophobic interactions with Trp^{145} and Tyr^{53} (*green*) of the AChBP, similar to those seen for [A10L,D14K]-PnIA. In contrast, Glu^{14} (*pink*) is solvent-exposed, and hence this residue is less likely to be crucial for receptor interactions compared with Pro^{6}.

expressed in oocytes must be dependent upon residues 10–15. Of these residues, Tyr^{10} (Vc1.1) *versus* Met^{10} (EpI) would appear to be the major cause of this difference, because a methionine in position 10 has been shown in PnIA to strongly favor interaction with the α7 subtype (35). In addition, mutation of Tyr^{15} to alanine in PnIB reduces activity at the α7 nAChR subtype by ~2-fold. Vc1.1 has an isoleucine in position 15 rather than the sulfated tyrosine present in EpI, and this may also contribute to the lack of activity of Vc1.1 on the α7 subtype.

Recently, the 4/3 α-conotoxin ImI has been shown to be a potent inhibitor of the α3β2 nAChR subtype when it was previously believed to be only selective for the homomeric α7 receptor (34, 40). ImI is identical in sequence to Vc1.1 (and EpI) from residues 1 through 8, and therefore the activity of ImI on α3β2 receptors is consistent with the activity profiles of Vc1.1 and EpI. Again, the difference in the second loops of ImI and Vc1.1 must explain the why ImI is active on the α7 nAChR subtype and Vc1.1 is not. ImI has only a short second loop (three residues), and it has been shown previously that Trp^{10} is important for biological activity (41). Replacement of Trp^{10} with threonine resulted in a 30-fold decrease in activity, whereas replacement with phenylalanine only reduced activity 3-fold suggesting that an aromatic residue is required at position 10. Mutation of residues 9 and 11 in ImI had little effect on activity at the α7 subtype (41). The x-ray structure of ImI bound to AChBP shows that Trp^{10} makes a number of contacts with the complementary binding side of the receptor at sites that the 4/7 α-conotoxin analogue [A10L,D14K]-PnIA does not (34). Vc1.1 has a tyrosine in position 10, which has an aromatic character yet also a hydroxyl group. It may be this hydroxyl group that is interfering with the interaction with the α7 receptor, or it may be a result of the longer second loop causing a disruption of the required interactions.

The structure-activity relationships of the 4/7 α-conotoxin MII have been studied in detail recently (42, 43). Interestingly, both MII and Vc1.1 act on α3β2 nAChR subtypes, but there are some significant differences in their activity profiles. MII is effective in the nanomolar range, has a greater selectivity for α3β2 than Vc1.1, but has a significantly lower potency for α3β4 subtypes. MII also has a greater potency for the α7 nAChR subtype, whereas Vc1.1 has minimal effect (44, 45). An alanine scan of MII showed that the mutations N5A, P6A, and H12A had a substantial effect on potency at the α3β2 and α6 nAChR subtypes, whereas H9A and L15A had more modest effects for α3β2 subtypes only (42, 43). Furthermore, mutation of His^{9}, Glu^{11}, and Leu^{15} to alanine has been shown to increase the selectivity of MII for α6-containing nAChRs (43). In addition to the highly conserved proline at position 6, some of the residues important for the activity of MII are mirrored in the sequence of Vc1.1. Both peptides have a negatively charged residue at position 11, Asp in Vc1.1 and Glu in MII, that may contribute to the selectivity of MII and Vc1.1 for the α3 subunit. MII and Vc1.1 also both have a histidine at position 12, and as the potency of MII was found to be pH-dependent, it has been suggested that this histidine is charged in the active form of the peptide (42). We have found that a reduction of pH increases the potency of Vc1.1, which supports the proposal that a protonated histidine may be important for the receptor interaction. Finally, the leucine at position 15 in MII is replaced with isoleucine in Vc1.1, which would have a similar hydrophobic interaction with the receptor. Therefore, the combined structure and activity data suggest that it is the N-terminal portion of Vc1.1 that is the major determinant of binding to the nAChR, with residues in the C-terminal portion of the molecule responsible for more subtle variations on potency and selectivity.

To our knowledge, this is the first report on the selectivity of Vc1.1 for nAChR subtypes. Vc1.1 had been assumed, based on the previously reported chromaffin cell binding studies, to be selective for α3β4-containing subtypes (6), and the involvement of the α5 subunit with α3β4 nAChRs had been speculated. We show that the potency of Vc1.1 was unchanged at α3α5β2 but exhibits a >5-fold reduction at α3α5β4 nAChRs relative to α3β4. The homomeric α7 nAChR exhibits <20% block in the presence of 30 μM Vc1.1. We have demonstrated that the post-translationally modified form of Vc1.1, vc1a, which is found in the venom, does not inhibit ACh-evoked currents mediated by any of the nAChR subtypes expressed in *Xenopus* oocytes. This is an interesting result from a biological viewpoint, because it implies that the cone snail is investing valuable metabolic energy into deactivating Vc1.1. However, it seems more likely that vc1a is produced to target an as yet unknown receptor target.

Finally, Vc1.1 has been reported to have an important contribution to the potential role of nAChRs in pain perception (8), because it is able to inhibit a vascular response to pain (6) and is able to reduce chronic pain in several animal models of human neuropathy (8, 9). Antagonists of nAChRs such as Vc1.1 might reduce the increase in axonal excitability produced by neuronal

nAChR activation (9). The structure reported here should open new opportunities for further development of Vc1.1 or analogues as analgesic agents.

Acknowledgments—We thank Drs. Bruce Livett and Charles Luetje for their critical review of the manuscript.

REFERENCES

1. Terlau, H., and Olivera, B. M. (2004) *Physiol. Rev.* **84,** 41–68
2. McIntosh, J. M., Santos, A. D., and Olivera, B. M. (1999) *Annu. Rev. Biochem.* **68,** 59–88
3. Adams, D. J., Alewood, P. F., Craik, D. J., Drinkwater, R. D., and Lewis, R. J. (1999) *Drug Dev. Res.* **46,** 219–234
4. Dutton, J. L., and Craik, D. J. (2001) *Curr. Med. Chem.* **8,** 327–344
5. Livett, B. G., Gayler, K. R., and Khalil, Z. (2004) *Curr. Med. Chem.* **11,** 1715–1723
6. Sandall, D. W., Satkunanathan, N., Keays, D. A., Polidano, M. A., Liping, X., Pham, V., Down, J. G., Khalil, Z., Livett, B. G., and Gayler, K. R. (2003) *Biochemistry* **42,** 6904–6911
7. Jakubowski, J. A., Keays, D. A., Kelley, W. P., Sandall, D. W., Bingham, J. P., Livett, B. G., Gayler, K. R., and Sweedler, J. V. (2004) *J. Mass Spectrom.* **39,** 548–557
8. Satkunanathan, N., Livett, B., Gayler, K., Sandall, D., Down, J., and Khalil, Z. (2005) *Brain Res.* **1059,** 149–158
9. Lang, P. M., Burgstahler, R., Haberberger, R. V., Sippel, W., and Grafe, P. (2005) *Neuroreport* **16,** 479–483
10. Lang, P. M., Burgstahler, R., Sippel, W., Irnich, D., Schlotter-Weigel, B., and Grafe, P. (2003) *J. Neurophysiol.* **90,** 3295–3303
11. Gayler, K., Sandall, D., Greening, D., Keays, D., Polidano, M., Livett, B., Down, J., Satkunanathan, N., and Khalil, Z. (2005) *IEEE Eng. Med. Biol. Mag.* **24,** 79–84
12. Schnölzer, M., Alewood, P., Jones, A., Alewood, D., and Kent, S. B. H. (1992) *Int. J. Pept. Protein Res.* **40,** 180–193
13. Guntert, P., Mumenthaler, C., and Wüthrich, K. (1997) *J. Mol. Biol.* **273,** 283–298
14. Brünger, A. T., Adams, P. D., and Rice, L. M. (1997) *Structure* **5,** 325–336
15. Linge, J. P., and Nilges, M. (1999) *J. Biomol. NMR* **13,** 51–59
16. Koradi, R., Billeter, M., and Wüthrich, K. (1996) *J. Mol. Graph.* **14,** 29–32, 51–55
17. Hutchinson, E. G., and Thornton, J. M. (1996) *Protein Sci.* **5,** 212–220
18. Laskowski, R. A., Rullmannn, J. A., MacArthur, M. W., Kaptein, R., and Thornton, J. M. (1996) *J. Biomol. NMR* **8,** 477–486
19. Lawrence, G. W., Weller, U., and Dolly, J. O. (1994) *Eur. J. Biochem.* **222,** 325–333
20. Fischer, H., Liu, D. M., Lee, A., Harries, J. C., and Adams, D. J. (2005) *J. Neurosci.* **25,** 3571–3577
21. Hogg, R. C., Hopping, G., Alewood, P. F., Adams, D. J., and Bertrand, D. (2003) *J. Biol. Chem.* **278,** 26908–26914
22. Arunlakshana, O., and Schild, H. O. (1959) *Br. J. Pharmacol.* **14,** 48–58
23. Celie, P. H., Kasheverov, I. E., Mordvintsev, D. Y., Hogg, R. C., van Nierop, P., van Elk, R., van Rossum-Fikkert, S. E., Zhmak, M. N., Bertrand, D., Tsetlin, V., Sixma, T. K., and Smit, A. B. (2005) *Nat. Struct. Mol. Biol.* **12,** 582–588
24. Abdrakhmanova, G., Cleemann, L., Lindstrom, J., and Morad, M. (2004) *Mol. Pharmacol.* **66,** 347–355
25. Nutter, T. J., and Adams, D. J. (1995) *J. Gen. Physiol.* **105,** 701–723
26. Livett, B., Khalil, Z., Gayler, K., and Down, J. (2002) Alpha conotoxin peptides with analgesic properties, patent WO 02/079236 A1
27. Hu, S. H., Loughnan, M., Miller, R., Weeks, C. M., Blessing, R. H., Alewood, P. F., Lewis, R. J., and Martin, J. L. (1998) *Biochemistry* **37,** 11425–11433
28. Hill, J. M., Oomen, C. J., Miranda, L. P., Bingham, J. P., Alewood, P. F., and Craik, D. J. (1998) *Biochemistry* **37,** 15621–15630
29. Shon, K. J., Koerber, S. C., Rivier, J. E., Olivera, B. M., and McIntosh, J. M. (1997) *Biochemistry* **36,** 15693–15700
30. Hu, S. H., Gehrmann, J., Alewood, P. F., Craik, D. J., and Martin, J. L. (1997) *Biochemistry* **36,** 11323–11330
31. Ellison, M., McIntosh, J. M., and Olivera, B. M. (2003) *J. Biol. Chem.* **278,** 757–764
32. Dutertre, S., Nicke, A., and Lewis, R. J. (2005) *J. Biol. Chem.* **280,** 30460–30468
33. Hansen, S. B., Sulzenbacher, G., Huxford, T., Marchot, P., Taylor, P., and Bourne, Y. (2005) *EMBO J.* **24,** 3635–3646
34. Ulens, C., Hogg, R. C., Celie, P. H., Bertrand, D., Tsetlin, V., Smit, A. B., and Sixma, T. K. (2006) *Proc. Natl. Acad. Sci. U. S. A.* **103,** 3615–3620
35. Quiram, P. A., McIntosh, J. M., and Sine, S. M. (2000) *J. Biol. Chem.* **275,** 4889–4896
36. Luo, S., Nguyen, T. A., Cartier, G. E., Olivera, B. M., Yoshikami, D., and McIntosh, J. M. (1999) *Biochemistry* **38,** 14542–14548
37. Broxton, N., Miranda, L., Gehrmann, J., Down, J., Alewood, P., and Livett, B. (2000) *Eur. J. Pharmacol.* **390,** 229–236
38. Nicke, A., Samochocki, M., Loughnan, M. L., Bansal, P. S., Maelicke, A., and Lewis, R. J. (2003) *FEBS Lett.* **554,** 219–223
39. Loughnan, M., Bond, T., Atkins, A., Cuevas, J., Adams, D. J., Broxton, N. M., Livett, B. G., Down, J. G., Jones, A., Alewood, P. F., and Lewis, R. J. (1998) *J. Biol. Chem.* **273,** 15667–15674
40. Ellison, M., Gao, F., Wang, H. L., Sine, S. M., McIntosh, J. M., and Olivera, B. M. (2004) *Biochemistry* **43,** 16019–16026
41. Quiram, P. A., and Sine, S. M. (1998) *J. Biol. Chem.* **273,** 11007–11011
42. Everhart, D., Cartier, G. E., Malhotra, A., Gomes, A. V., McIntosh, J. M., and Luetje, C. W. (2004) *Biochemistry* **43,** 2732–2737
43. McIntosh, J. M., Azam, L., Staheli, S., Dowell, C., Lindstrom, J. M., Kuryatov, A., Garrett, J. E., Marks, M. J., and Whiteaker, P. (2004) *Mol. Pharmacol.* **65,** 944–952
44. Cartier, G. E., Yoshikami, D., Gray, W. R., Luo, S., Olivera, B. M., and McIntosh, J. M. (1996) *J. Biol. Chem.* **271,** 7522–7528
45. Kuryatov, A., Olale, F., Cooper, J., Choi, C., and Lindstrom, J. (2000) *Neuropharmacology* **39,** 2570–2590
46. Fainzilber, M., Hasson, A., Oren, R., Burlingame, A. L., Gordon, D., Spira, M. E., and Zlotkin, E. (1994) *Biochemistry* **33,** 9523–9529
47. McIntosh, J. M., Dowell, C., Watkins, M., Garrett, J. E., Yoshikami, D., and Olivera, B. M. (2002) *J. Biol. Chem.* **277,** 33610–33615
48. Nicke, A., Loughnan, M. L., Millard, E. L., Alewood, P. F., Adams, D. J., Daly, N. L., Craik, D. J., and Lewis, R. J. (2003) *J. Biol. Chem.* **278,** 3137–3144
49. McIntosh, J. M., Yoshikami, D., Mahe, E., Nielsen, D. B., Rivier, J. E., Gray, W. R., and Olivera, B. M. (1994) *J. Biol. Chem.* **269,** 16733–16739
50. Wishart, D. S., Bigam, C. G., Holm, A., Hodges, R. S., and Sykes, B. D. (1995) *J. Biomol. NMR* **5,** 67–81

The Synthesis, Structural Characterization, and Receptor Specificity of the α -Conotoxin Vc1.1

Richard J. Clark, Harald Fischer, Simon T. Nevin, David J. Adams and David J. Craik

J. Biol. Chem. 2006, 281:23254-23263.
doi: 10.1074/jbc.M604550200 originally published online June 5, 2006
